ACS NANO

www.acsnano.org

ARTICLE

Confined Cascade Metabolic Reprogramming Nanoreactor for Targeted Alcohol Detoxification and Alcoholic Liver Injury Management

Xudong Geng,[#] Xuancheng Du,[#] Weijie Wang, Chengmei Zhang, Xiangdong Liu, Yuanyuan Qu, Mingwen Zhao, Weifeng Li, Mingzhen Zhang, Kangsheng Tu,[*] and Yong-Qiang Li[*]

Cite This: *ACS Nano* 2023, 17, 7443−7455

Read Online

ACCESS | Metrics & More | Article Recommendations | Supporting Information

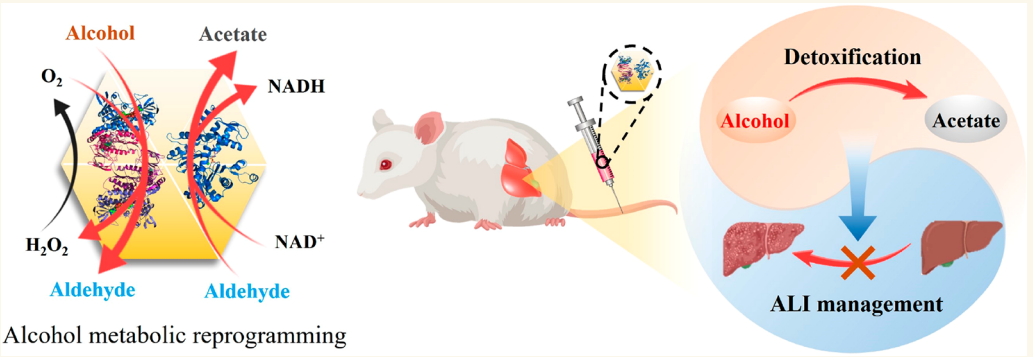

Alcohol metabolic reprogramming

ABSTRACT: **Alcoholic liver injury (ALI) is the leading cause of serious liver disease, whereas current treatments are mostly supportive and unable to metabolize alcohol directly. Here we report a metabolic reprogramming strategy for targeted alcohol detoxification and ALI management based on a confined cascade nanoreactor. The nanoreactor (named AA@mMOF) is designed by assembling natural enzymes of alcohol oxidase (AOx) and aldehyde dehydrogenase (ALDH) in the cavity of a mesoporous metal organic framework (mMOF) nanozyme with intrinsic catalase (CAT)-like activity. By conducting confined AOx/CAT/ALDH cascade reactions, AA@mMOF enables self-accelerated alcohol degradation (>0.5 $mg{\cdot}mL^{-1}{\cdot}h^{-1}$) with negligible aldehyde diffusion and accumulation, reprogramming alcohol metabolism and allowing high-efficiency detoxification. Administered to high-dose alcohol-intoxicated mice, AA@mMOF shows surprising liver targeting and accumulation performance and dramatically reduces blood alcohol concentration and rapidly reverses unconsciousness and acute liver injury to afford targeted alcoholism treatment. Moreover, AA@mMOF dramatically alleviates fat accumulation and oxidative stress in the liver of chronic alcoholism mice to block and reverse the progression of ALI. By conducting confined AOx/CAT/ALDH cascade reactions for high-efficiency alcohol metabolism reprogramming, AA@mMOF nanoreactor offers a powerful modality for targeted alcohol detoxification and ALI management. The proposed confined cascade metabolic reprogramming strategy provides a paradigm shift for the treatment of metabolic diseases.**

KEYWORDS: *alcoholism, alcoholic liver injury, confined cascade catalysis, metabolic reprogramming, nanozymes*

INTRODUCTION

Alcoholism is a serious health risk factor that leads to a range of gastrointestinal and hepatic disorders.[1,2] In particular, alcoholic liver injury (ALI) including fibrosis, hepatitis, cirrhosis, and hepatic carcinoma accounts for nearly 6% of all death globally and has been recognized as a worldwide

Received: December 5, 2022
Accepted: April 12, 2023
Published: April 14, 2023

https://doi.org/10.1021/acsnano.2c12075
ACS Nano 2023, 17, 7443−7455

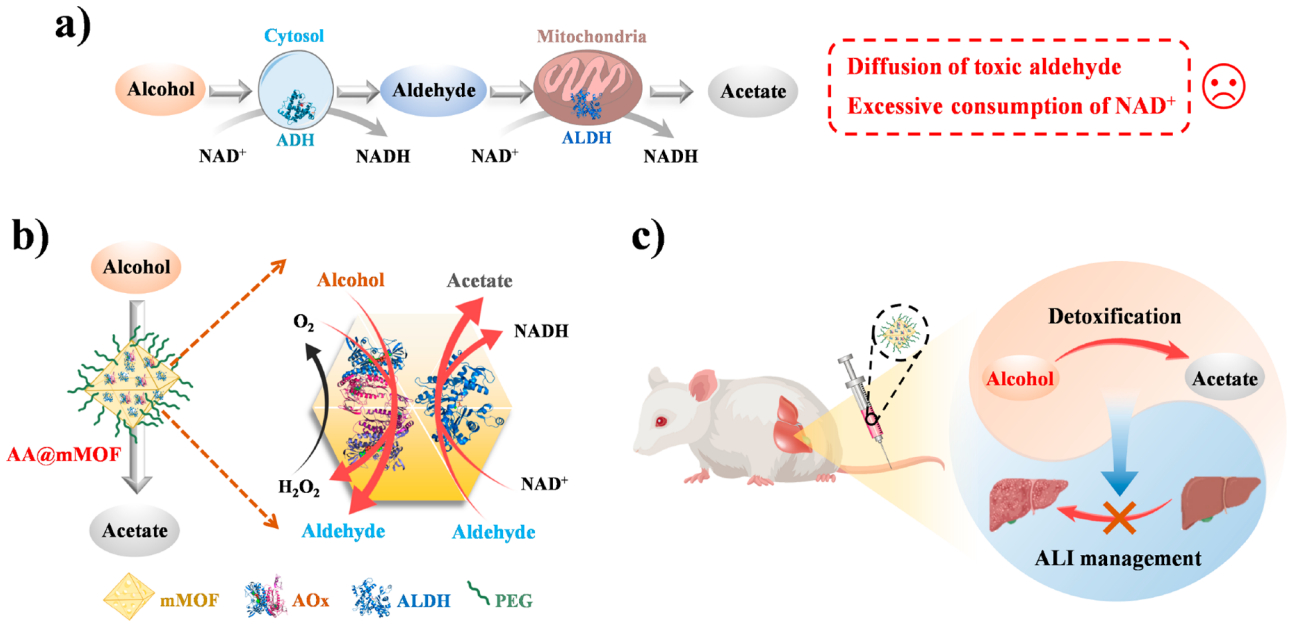

Figure 1. Schematic illustration of the design of confined cascade metabolic reprogramming nanoreactor for targeted alcohol detoxification and ALI management. (a) Alcohol metabolism pathway in hepatocytes. (b) Reprogramming of alcohol metabolism in AA@mMOF nanoreactor via confined cascade AOx/CAT/ALDH reaction. (c) AA@mMOF nanoreactor for *in vivo* alcohol detoxification and ALI management.

heath priority by the World Health Organization (WHO).[3−5] Alcohol detoxification is a prerequisite and critical for the management of ALI. Current treatments extensively used in clinical practice for alcohol intoxication including gastrointestinal mucosa protection, gastric lavage, and hemodialysis are primarily supportive and have a minor detoxification effect due to their inability to directly metabolize alcohol.[6,7] The metabolism of alcohol *in vivo* mainly relies on cytosolic alcohol dehydrogenase (ADH) and mitochondrial aldehyde dehydrogenase (ALDH) in hepatocytes (Figure 1a).[8,9] The ADH/ALDH system synergistically degrades alcohol into acetate via consecutive reactions and achieves effective alcohol metabolism. However, the expression of ADH and ALDH is relatively insufficient especially in Asian populations to degrade excess alcohol in alcoholism.[10] In addition, the ADH/ALDH cascade reaction consumes a substantial amount of energy metabolism cofactor of nicotinamide adenine dinucleotide (NAD^+), disrupting cellular energy homeostasis to result in cellular damage and senescence.[11] What's more, the spatially separated cytosolic ADH/mitochondrial ALDH metabolic system easily causes the diffusion of a toxic intermediate of aldehyde, inducing oxidative stress that causes structural and functional damage of the liver.[12] Moreover, alcohol metabolism is affected and reduced by other types of dependence such as illicit drugs, junk food, and smoking, due to enzymatic interference and their pharmacokinetic interactions with alcohol occurring in the liver, exacerbating the progression of ALI.[13] To address these issues, confined catalytic systems with alcohol metabolic reprogramming capability are highly desired.

The microsomal ethanol oxidizing system (MEOS) can catalyze the oxidation of alcohol into aldehyde via alcohol oxidase (AOx) without the consumption of NAD^+,[14] and the generated aldehyde is then decomposed into acetate by ALDH, offering an alternative pathway for alcohol metabolism. However, MEOS is normally disabled *in vivo* due to the production of toxic byproduct of H_2O_2 as well as the requirement of high O_2 supply in AOx-dependent alcohol oxidation, and only becomes active when the body is exposed to a lethal dose of alcohol.[15,16] By assembling enzymes with complementary functions to form multienzyme architectures, nature ingeniously solves the issue of toxic intermediates via confined cascade catalysis, in which toxic metabolic intermediates generated by one enzyme can be promptly eliminated by colocalized complementary enzyme.[17,18] Catalase (CAT) enables the decomposition of H_2O_2 into O_2, having the capability to simultaneously solve the problem of toxic H_2O_2 accumulation and O_2 supply in the process of AOx-based alcohol degradation.[19−21] It is conceivable that the construction of confined AOx/CAT/ALDH cascade system would afford an opportunity for alcohol metabolic reprogramming to tackle alcoholism. Metal organic frameworks (MOFs), a class of porous materials synthesized by metal-containing nodes and organic linkers, are emerging as a reliable carrier for enzymatic cascade systems,[22−24] because their porous cavity can protect enzymes from structural degradation/deactivation and ensure higher loading and easy mobility of substrates to achieve efficient catalytic effect. In addition, the presence of metal-containing nodes contributes potential active sites for catalysis, thus endowing MOFs with intrinsic enzyme-like activity.[25,26] More importantly, MOFs can be easily captured by the reticuloendothelial system (RES), possessing an innate liver-targeting capability.[27,28] Therefore, we hypothesize that by employing MOFs as both CAT mimic and carrier of natural enzymes of AOx and ALDH to catalyze confined AOx/CAT/ALDH cascade reactions, a robust strategy for targeted alcohol metabolic reprogramming could be developed.

Herein, we report a confined cascade metabolic reprogramming nanoreactor for targeted alcohol detoxification and ALI management (Figure 1b). This nanoreactor (termed AA@mMOF) is fabricated by incorporating mesoporous Fe-containing MIL-101 MOF (mMOF) with natural enzymes of AOx and ALDH and then encapsulating it with polyethylene

https://doi.org/10.1021/acsnano.2c12075
ACS Nano 2023, 17, 7443−7455

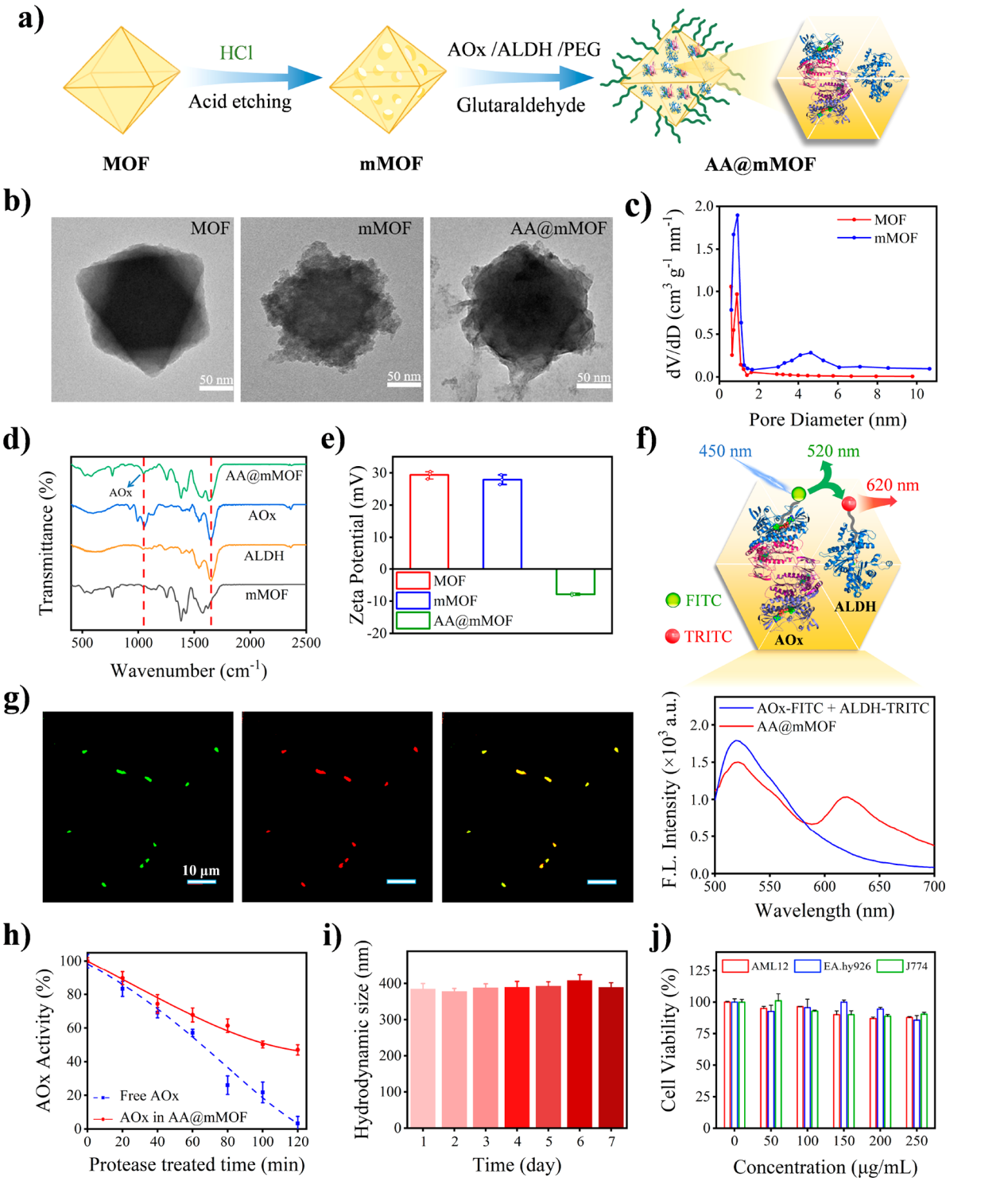

Figure 2. Characterization of AA@mMOF nanoreactor. (a) Schematic illustration of AA@mMOF preparation. (b) Representative TEM images of MOF, mMOF, and AA@mMOF. (c) Pore size distribution of MOF and mMOF. (d) FTIR spectra of mMOF, AOx, ALDH, and AA@mMOF. (e) ζ potentials of MOF, mMOF, and AA@mMOF. (f) Schematic illustration of the FRET between AOx-FITC and ALDH-TRITC in AA@mMOF (top), and the fluorescence spectra of the mixture of AOx-FITC and ALDH-TRITC as well as the corresponding AA@mMOF under 450 nm excitation (down). (g) Confocal fluorescence microscopy images of AA@mMOF under 488 nm excitation to demonstrate the colocalization of AOx-FITC and ALDH-TRITC. (h) Variation curve of AOx activity of AA@mMOF with treatment time of protease. (i) Hydrodynamic diameters of AA@mMOF in PBS buffer (0.01 M, pH7.4) during 1 week of storage. (j) Viability of the human umbilical vein cells (EA.hy926), mouse mononuclear macrophages (J774), and mouse normal liver cells (AML12) after incubation with AA@mMOF at various concentrations for 24 h, respectively. In (e) and (h−j), the values of ζ potential, AOx activity, hydrodynamic diameter, and cell viability represent the mean of three independent experiments, and the error bars indicate the standard deviation (SD) from the mean.

https://doi.org/10.1021/acsnano.2c12075
ACS Nano 2023, 17, 7443−7455

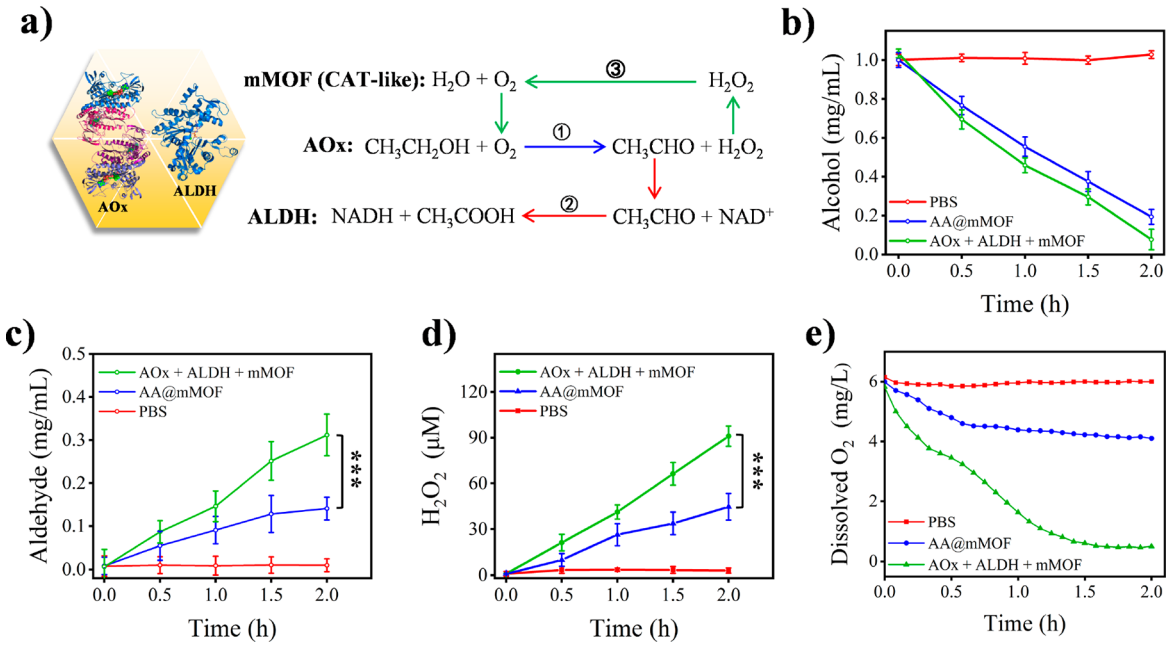

Figure 3. Alcohol metabolism pathway in AA@mMOF nanoreactor. (a) Schematic illustration of confined cascade AOx/CAT/ALDH reaction in AA@mMOF for alcohol metabolism. The curve of alcohol degradation (b), aldehyde accumulation (c), H_2O_2 elimination (d), and O_2 generation (e) in alcohol solution (1 mg/mL) incubated with AA@mMOF for 2 h. The groups of PBS and separated catalytic system were used as the control, and small amounts of NAD^+ (100 μg/mL) were added in all groups. In (b−e), the concentration values of ethanol, aldehyde, H_2O_2, and O_2 represent the mean of three independent experiments, and the error bars indicate the SD from the mean. ***P < 0.001.

glycol (PEG) shell. The mesoporous structure (porous size around 6 nm) of mMOF provides an abundant immobilization site and sufficient protection for AOx and ALDH to allow efficient oxidative degradation of alcohol without excessive consumption of NAD^+ and forms confined reaction environments to significantly enhance the local concentration of substrates and overall catalysis efficiency. Meanwhile, Fe-containing nodes of mMOF bestow the AA@mMOF with CAT-like activity to eliminate the toxic H_2O_2 byproduct generated in AOx-based alcohol oxidation and produce O_2 to turn waste into wealth,[29] realizing high-efficiency alcohol metabolic reprogramming via AOx/CAT/ALDH cascade reactions. Moreover, the confined architecture of liver-targeted AA@mMOF minimizes the diffusion of harmful intermediates of aldehyde (the leading culprit of ALI) and allows it to be promptly degraded by the proximate ALDH,[30,31] significantly reducing the occurrence and progression of ALI. By ingeniously reprogramming alcohol's metabolism via confined cascade catalysis, the AA@mMOF nanoreactor may offer a powerful paradigm for clinical alcohol detoxification and ALI management (Figure 1c). Compared to current clinical alcoholism antidotes that are mostly supportive and unable to metabolize alcohol directly, the proposed confined cascade metabolic reprogramming strategy provides a paradigm shift for high-efficiency management of alcoholism-associated serious diseases.

RESULTS AND DISCUSSION

Preparation and Characterization of AA@mMOF Nanoreactor. In typical experiments, the Fe-containing MIL-101 MOF was first synthesized using a solvothermal method followed by acid etching to yield mMOF with mesoporous structure,[32,33] and the AA@mMOF nanoreactor was then prepared by sequential AOx/ALDH covalent loading and PEG modification (Figure S1 and Figure 2a).[34] The transmission electron microscopy (TEM) images showed that the prepared MOF had a well-defined octahedral structure with an average size of 197 nm, and its pore size was found to be broadened from micropore (less than 2 nm) to mesoporous (around 6 nm) after acid etching based on the N_2 adsorption−desorption experiments (Figure 2b,c and Figure S2). In addition, similar X-ray powder diffraction (XRD) patterns were observed for MOF before and after etching (Figure S3). This phenomenon indicated that acid etching is a feasible method to significantly increase the pore size of MOF for subsequent enzyme loading without damaging the basic crystal structure. The covalent loading of AOx/ALDH could be confirmed by the Fourier transform infrared (FTIR) spectrum of AA@mMOF in which the characteristic peak of AOx was clearly found (Figure 2d). The loading amount of AOx/ALDH (426.1 ± 35 μg of AOx/ALDH per mg of mMOF) was quantitatively determined by bicinchoninic acid (BCA) assay (Figure S4).[35] Moreover, the whole preparation process of AA@mMOF could also be monitored and confirmed by the reversed ζ potential and increased hydrodynamic size results (Figure 2e and Figure S5).

The confined architecture of MOF spatially locates the AOx and ALDH within close proximity. To confirm this, Förster resonance energy transfer (FRET) assay was carried out using fluorescein isothiocyanate (FITC)-labeled AOx (AOx-FITC) and tetramethylrhodamine B (TRITC)-labeled ALDH (ALDH-TRITC) as the constituent enzymes. Figure 2f showed the fluorescence spectra of a mixture of the two constituent enzymes (AOx-FITC+ALDH-TRITC, equal molar ratio) as well as the corresponding AA@mMOF. Because FITC and TRITC have excitation maxima at 490 and 550 nm,[36] respectively, the mixture of AOx-FITC and ALDH-TRITC only exhibited FITC emission centered at 520 nm when under

https://doi.org/10.1021/acsnano.2c12075
ACS Nano 2023, 17, 7443−7455

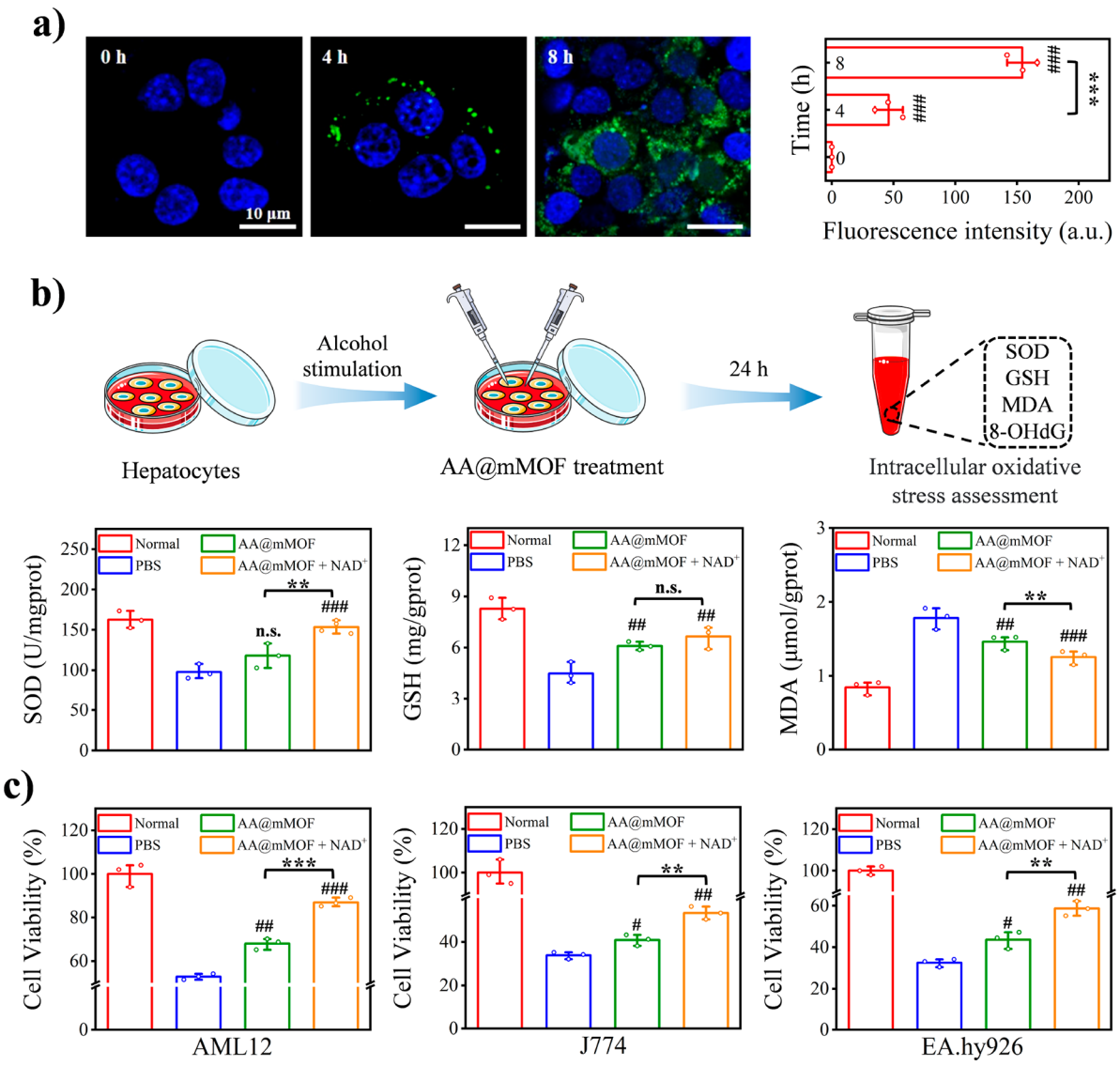

Figure 4. ***In vitro*** **alcohol detoxification performance of AA@mMOF nanoreactor. (a) Representative overlapping CLSM images and corresponding fluorescence intensities of AML12 cells incubated with AA@mMOF at various time points. The group of 0 h was used as the positive control. (b) Schematic illustration and experimental data (SOD activity, GSH and MDA concentration) of intracellular oxidative stress assessment of alcohol-stimulated AML12 hepatocytes in different treatment groups. (c) Viability of alcohol-stimulated AML12, J774, and EA.hy926 cells in different treatment groups, respectively. In (b) and (c), the group of PBS treatment was used as the positive control, and the group of normal cells without alcohol stimulation was used as the negative control. In (a−c), the values of fluorescence intensity, SOD activity, GSH and MDA concentration, and cell viability represent the mean of three independent experiments, and the error bars indicate the SD from the mean. # indicates the contrast between experimental group and positive control. $^{\#}P < 0.05$, $^{\#\#}/^{**}P < 0.01$, $^{\#\#\#}/^{***}P < 0.001$, and $^{n.s.}P > 0.05$.**

450 nm excitation. In sharp contrast, AA@mMOF possessed intense emissions from both FITC and TRITC (centered at 520 and 620 nm, respectively) under 450 nm excitation, demonstrating the occurrence of FRET from FITC to TRITC and confirming the short distance (<10 nm) between AOx and ALDH (Figure 2f).[37] The corresponding confocal fluorescence microscope images showed a consistent phenomenon in which colocalization of green (FITC) and red (TRITC) fluorescence was only observed in AA@mMOF under 488 nm laser excitation, further proving the close association of AOx and ALDH in nanoreactor (Figure 2g and Figure S6). The loading amount of AOx and ALDH in nanoreactor was calculated to be 119.70 ± 9.77 μg and 330.37 ± 10.26 μg per mg of mMOF, respectively, based on the standard fluorescence intensity curves of AOx-FITC and ALDH-TRITC (Figure S7). In addition, AA@mMOF was found to possess extremely low release rate of enzymes over time and retain much higher enzymatic activity under different adverse environmental influences (protease, weak acid, and heat) compared to natural enzymes, indicating the covalent binding of enzymes and strong protective effect of MOF on the loaded enzymes (Figure 2h, Figures S8 and S9). Furthermore, the prepared AA@mMOF were demonstrated to exhibit long-time size stability and outstanding biocompatibility based on the results of dynamic light scattering measurement, CCK-8 assay and hemolysis test (Figure 2i,j and Figure S10). This excellent size stability and biocompatibility may be attributed to the PEG modification on the surface of AA@mMOF.[38] As an effective

https://doi.org/10.1021/acsnano.2c12075
ACS Nano 2023, 17, 7443−7455

antioxidant, the MIL-101 MOF exhibits intrinsic CAT-like activity due to existence of Fe^{3+} node.[29,39] X-ray photoelectron spectroscopy (XPS) analysis identified the presence of Fe^{3+} in AA@mMOF, heralding the potential CAT-like capability of nanoreactor to turn the toxic H_2O_2 waste into valuable O_2 (Figure S11).

Alcohol Metabolism Pathway in AA@mMOF Nanoreactor. The close association of AOx and ALDH in AA@mMOF with CAT-like activity forms a three-step catalytic system for alcohol metabolism via confined AOx/CAT/ALDH cascade reaction (Figure 3a). First, the loaded AOx catalyzes the oxidation of alcohol into aldehyde accompanied by the generation of H_2O_2 byproduct without the consumption of NAD^+ cofactor (step 1). The toxic aldehyde intermediates are then promptly converted into acetic acid by the colocalized ALDH to avoid the oxidative stress damage caused by aldehyde diffusion (step 2). Meanwhile, the nocuous H_2O_2 byproduct can be rapidly eliminated by the intrinsic CAT-like activity of mMOF, and vast amounts of oxygen are also produced in this process which in turn accelerates AOx catalysis process and creates a virtuous cycle for alcohol metabolism (step 3). The optimal pH values for AOx, ALDH and CAT-like activity of mMOF were all found to be around 7.5, which matches the pH of the extracellular environment in mice and is conducive to the degradation of alcohol (Figure S12).[40] To verify the aforementioned alcohol metabolism pathway in nanoreactor, an alcohol solution that meet the criteria for drunk driving (1 mg/mL) was mixed with AA@mMOF,[41] and its metabolism process was analyzed by monitoring the degradation of alcohol, the accumulation of aldehyde, the elimination of H_2O_2, and the generation of O_2 in real time. As shown in Figure 3b, AA@mMOF nanoreactor catalyzed the conversion of more than 80% of alcohol in 2 h, possessing outstanding alcohol degradation capability. In addition, similar alcohol degradation curves were observed in AA@mMOF and the separated catalytic system (AOx + ALDH + mMOF), indicating that the covalent loading of AOx in nanoreactor has negligible effect on its catalytic efficiency. Moreover, much lower accumulation rate of the aldehyde intermediate was obtained in AA@mMOF within 2 h compared to the separated catalytic system, demonstrating significantly enhanced AOx/ALDH reaction efficiency in the confined architecture of nanoreactor (Figure 3c and Figure S13). Furthermore, AA@mMOF realized enhanced elimination of H_2O_2 byproduct and generation of O_2 via confined AOx/CAT reaction, simultaneously solving the issues of toxic H_2O_2 accumulation and O_2 consumption occurred in AOx-based alcohol degradation (Figure 3d,e). The confirmed performance of fast alcohol degradation and inhibited aldehyde accumulation as well as the enhanced H_2O_2 elimination and massive O_2 production demonstrate the feasibility of AA@mMOF nanoreactor for alcohol metabolism reprogramming.

***In Vitro* Alcohol Detoxification.** The robust alcohol metabolic reprogramming capability of AA@mMOF nanoreactor makes it a promising antidote for alcohol intoxication. Considering that hepatocytes are the primary site of alcohol metabolism,[42] the AA@mMOF nanoreactor was incubated with alpha mouse liver 12 (AML12) hepatocytes, and its cell uptake and the performance for *in vitro* alcohol detoxification were investigated. Figure 4a showed the confocal laser scanning microscopy (CLSM) images and corresponding fluorescence intensities of AML12 cells incubated with AA@mMOF at various time points. It was found that the fluorescence of AA@mMOF (coming from loaded AOx-FITC) in AML12 cells was obvious after 4 h incubation and continued to increase with the extension of incubation time, demonstrating wonderful hepatocyte uptake efficiency. Subsequently, the cellular uptake mechanism of AA@mMOF was investigated in the presence of different inhibitors. Herein, the inhibitors of cytochalasin D, chlorpromazine (CPZ), methyl-β-cyclodextrin (M-β-CD) and ethylisopropyl amiloride (EIPA) were employed to inhibit the process of phagocytosis, clathrin-mediated endocytosis (CME), caveolae-mediated endocytosis (CvME) and micropinocytosis, respectively. As shown in Figures S14 and S15, the intracellular fluorescence intensity (coming from loaded AOx-FITC) and Fe content were significantly reduced in AML 12 cells treated with M-β-CD and EIPA compared to that treated with cytochalasin D and CPZ. This phenomenon demonstrated that AA@mMOF enters the liver cell mainly through CvME and micropinocytosis rather than CME and phagocytosis. Moreover, the intracellular localization of AA@mMOF was analyzed based on a colocalization assay of nanoreactor and endosome/lysosome. From Figure S16, it was found that only a portion of AA@mMOF (with red fluorescence coming from loaded ALDH-TRITC) was colocalized with endosome/lysosome (labeled by LysoTracker green), indicating that the nanoreactors were distributed in both lysosomes and cytoplasm. This intracellular distribution makes AA@mMOF less susceptible to lysosomal degradation and allows efficient use of the high concentration of NAD^+ in the cytoplasm to achieve high-efficiency intracellular alcohol degradation.

To perform intracellular alcohol detoxification experiment, alcohol-stimulated AML12 cells were treated by AA@mMOF, and intracellular oxidative stress status was examined. As shown in Figure 4b and Figure S17, compared to normal AML12 cells, significantly reduced antioxidant capacity characterized by decreased superoxide dismutase (SOD) activity and glutathione (GSH) concentration[43] and greatly enhanced oxidative damage of biomacromolecules reflected by increased generation of malondialdehyde (MDA) and 8-hydroxydeoxyguanosine (8-OHdG)[44,45] were observed in alcohol-stimulated AML12 cells in the treatment group of PBS (control), indicating the occurrence of serious intracellular oxidative stress. In sharp contrast, improved intracellular SOD activity and GSH concentration as well as decreased MDA and 8-OHdG generation were obtained in the treatment group of AA@mMOF, confirming the outstanding intracellular oxidative stress relieving capability of nanoreactor. In addition, the treatment group of AA@mMOF plus NAD^+ was found to exhibit a relatively stronger oxidative stress relieving performance than AA@mMOF, which is probably related to the enhanced ALDH catalytic efficiency of nanoreactor in the condition of high NAD^+ concentration (the sum of intracellular and exogenous addition).[46] The alleviated level of intracellular oxidative stress will inevitably improve the survival of hepatocytes.[47] As shown in Figure 4c, compared to the control group (PBS treatment), much higher cell viability of alcohol-stimulated AML12 hepatocytes was obtained after nanoreactor treatment especially in the group of AA@mMOF plus NAD^+ (around 85%). In addition to hepatocytes, AA@mMOF also vastly improved the survival of alcohol-stimulated mouse mononuclear macrophages (J774) and human umbilical vein cells (EA.hy926), exhibiting broad-spectrum intracellular alcohol detoxification capability independent of cell types (Figure 4c).

https://doi.org/10.1021/acsnano.2c12075
ACS Nano 2023, 17, 7443−7455

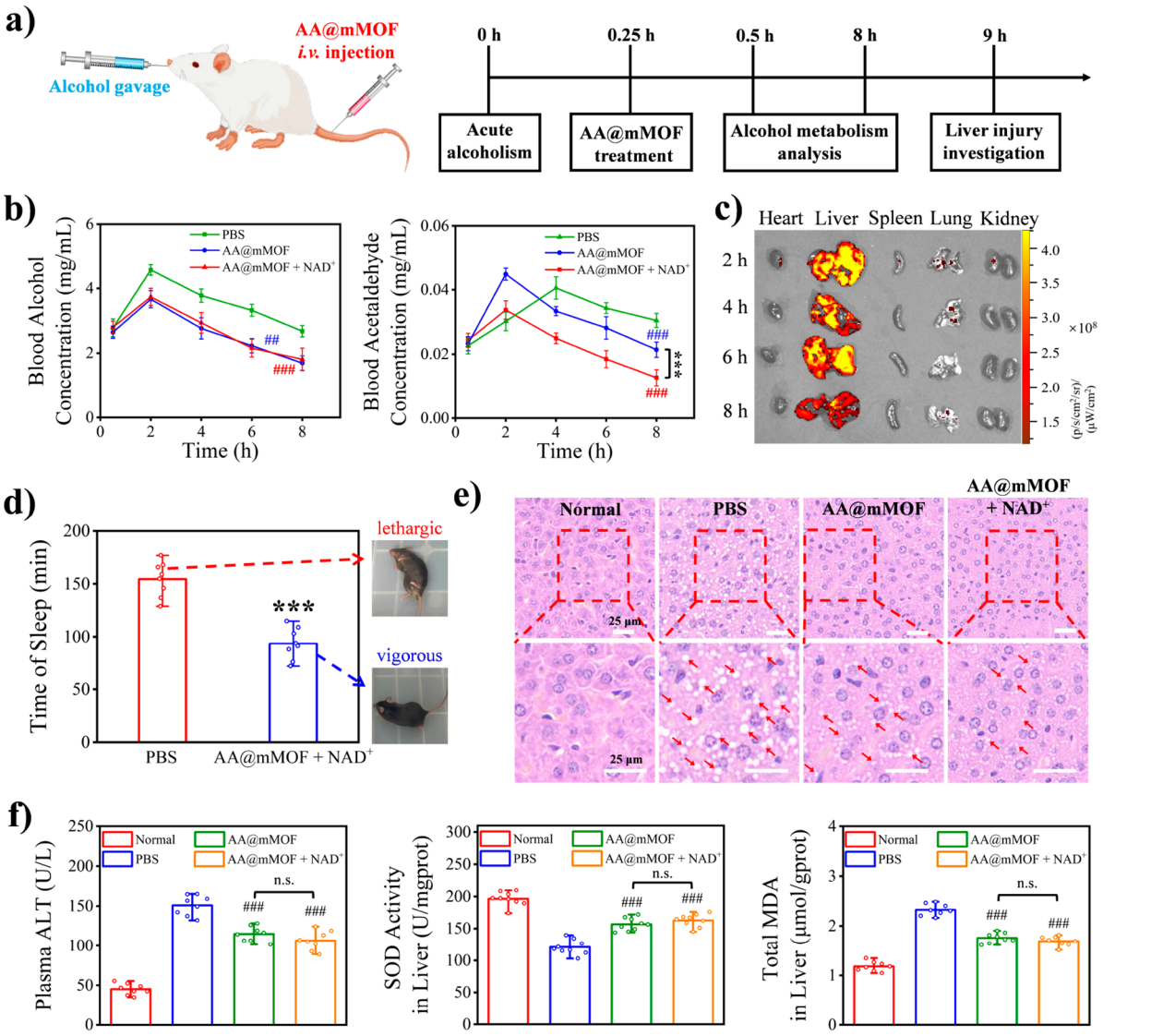

Figure 5. ***In vivo*** **performance of AA@mMOF nanoreactor for acute alcoholism treatment in C57BL/6J mice. (a) Schematic illustration and experimental timeline of AA@mMOF for** ***in vivo*** **treatment of acute alcoholism. (b) The change curves of blood concentrations of alcohol and aldehyde in different treatment groups. (c)** ***Ex vivo*** **tissue fluorescence images of intoxicated mice intravenously injected with AA@mMOF at different time points postgavage to indicate the distribution of nanoreactor** ***in vivo*****. The fluorescence comes from the ALDH-TRITC loaded in nanoreactor. (d) The righting reflex test and corresponding quantitative sleep time data of the intoxicated mice treated by PBS and AA@mMOF plus NAD^+, respectively. (e) Representative H&E staining images of the liver of intoxicated mice in different treatment groups at 9 h postgavage. (f) Plasma ALT level, liver SOD activity, and liver MDA concentration of intoxicated mice in different treatment groups at 9 h postgavage. In (b), (d), (e), and (f), the treatment group of PBS was used as the positive control, while the group of normal healthy mice was used as the negative control. In (b), (d), and (f), the values of blood alcohol/aldehyde concentration, sleep time, plasma ALT concentration, and liver SOD activity and MDA concentration represent the mean of eight independent experiments, and the error bars indicate the SD from the mean. # indicates the contrast between experimental group and positive control. $^{*}P < 0.05$, $^{\#\#}P < 0.01$, $^{\#\#\#/***}P < 0.001$, $^{n.s.}P > 0.05$.**

In Vivo **Treatment of Acute Alcoholism.** By rapidly degrading alcohol and reducing intracellular oxidative stress, the AA@mMOF nanoreactor provides an effective tool for *in vivo* alcoholism treatment. To confirm this, a mouse model of acute alcoholism was constructed.[48] AA@mMOF was then intravenously injected into the intoxicated mice, and its therapeutic performance for alcoholism was evaluated based on alcohol metabolism analysis, righting reflex test, and live injury investigation (Figure 5a and Figure S18a). Figure 5b and Figure S18b show the real-time change curves of blood alcohol and aldehyde concentration within 8 h treatment. It was found that blood concentrations of alcohol and aldehyde of intoxicated mice were both significantly reduced in the treatment group of AA@mMOF compared to control (PBS), demonstrating that *in vivo* alcohol metabolism was greatly enhanced by the nanoreactor via faster alcohol degradation and aldehyde elimination. In addition, the performance of the nanoreactor for blood aldehyde elimination was further improved by exogenous addition of NAD^+ due to enhanced ALDH catalytic efficiency in the condition of high NAD^+ concentration (Figure 5b and Figure S18b). It should be emphasized that such excellent alcohol metabolism performance of the nanoreactor is not only due to its architecture to perform confined AOx/CAT/ALDH cascade reactions but

https://doi.org/10.1021/acsnano.2c12075
ACS Nano 2023, 17, 7443−7455

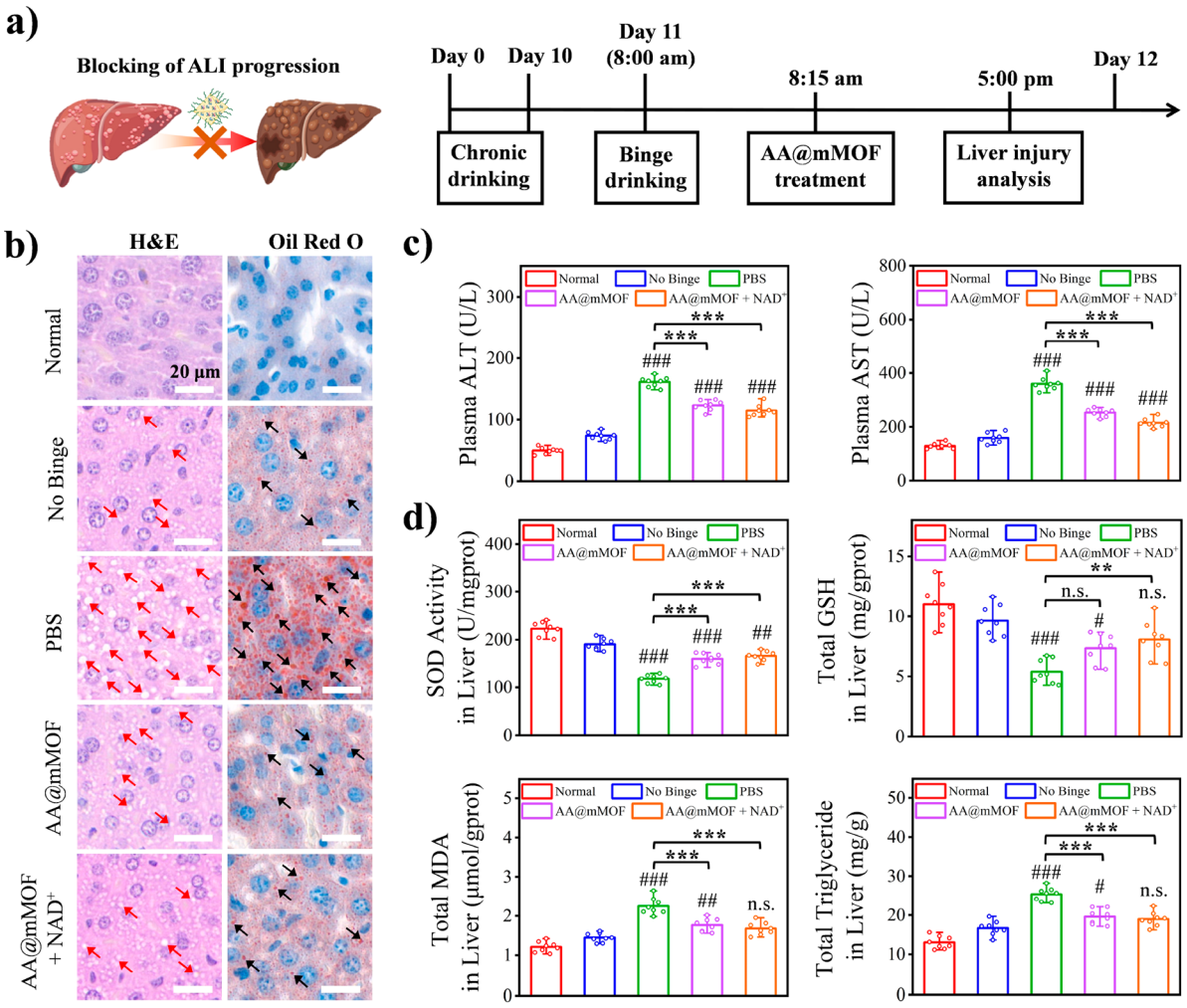

Figure 6. ***In vivo*** **performance of AA@mMOF nanoreactor for ALI management in C57BL/6J mice. (a) Schematic illustration and experimental timeline of AA@mMOF for** ***in vivo*** **ALI management. Representative liver H&E and Oil Red O staining images (b), the concentrations of plasma ALT and AST (c), and liver oxidative stress level characterized by SOD activity, and total concentrations of GSH, MDA and triglyceride (d) of ALI mice in different treatment groups. The group of PBS and no binge was used as the positive and negative control, respectively. In (c) and (d), the values of plasma ALT and AST concentration, SOD activity, the concentration of GSH, MDA and triglyceride represent the mean of eight independent experiments, and the error bars indicate the SD from the mean. # indicates the contrast between experimental group and negative control.** $^{\#/*}P < 0.05$, $^{\#\#/**}P < 0.01$, $^{\#\#\#}P < 0.001$, $^{n.s.}P > 0.05$.

also may be closely related to its innate liver-targeting capability *in vivo*.[49] The slow blood flow rate in the hepatic sinusoids (about half of the blood flow rate of capillaries) will theoretically prolong the residence time of AA@mMOF in the liver and increase the contact between liver cells and nanoreactors.[50] Meanwhile, the larger particle size of AA@mMOF will make it easier to be trapped by the Kupfer cells in the hepatic blood sinusoids, allowing superior *in vivo* liver targeting.[51] As shown in Figure 5c and Figure S19, AA@mMOF was efficiently taken up by hepatocytes and Kupfer cells and exhibited superior *in vivo* liver targeting and long-term resident properties, which means that the nanoreactor can be rapidly transported to the liver where it collaborates with existing ADH/ALDH system to achieve synergistic alcohol metabolism.

Subsequently, the righting reflex test, a gold standard for assessing arousal level in rodents with a range of neurological disorders,[52] was employed to investigate the recovery of consciousness of intoxicated mice after treatment. As shown in Videos S1 and S2, Figure 5d and Figure S18d, the intoxicated mice treated by AA@mMOF plus NAD^+ regained consciousness quickly, and showed much shorter sleep time (93 min vs 154 min in C57BL/6J mice, and 80 min vs 140 min in Balb/c mice) than the control (PBS treatment), showing a surprising ability to recover from alcohol intoxication. In addition to unconsciousness, live injury is the most common adverse effect of alcoholism.[53] Therefore, a systematic analysis for the live injury of intoxicated mice after treatment was further conducted. H&E staining images of liver tissues taken from the intoxicated mice at 9 h postgavage showed that the formation of lipid droplets (red arrows) was significantly inhibited in the treatment groups of AA@mMOF and AA@MOF plus NAD^+ compared to control (PBS), indicating mitigated histopathological damage of liver after nanoreactor treatment (Figure 5e and Figure S18e). In addition, intoxicated mice after AA@mMOF treatment possessed much lower blood concentrations of alanine aminotransferase (ALT) and aspartate aminotransferase (AST) than the control group, demonstrating relatively mild liver function impairment (Figure 5f, Figures S18f, S20, and S21). Moreover, the level

https://doi.org/10.1021/acsnano.2c12075
ACS Nano 2023, 17, 7443−7455

of liver oxidative stress of intoxicated mice was greatly relieved after nanoreactor treatment based on the results of SOD activity evaluation and GSH/MDA/8-OHdG measurement (Figure 5f, Figures S18f, S22, and S23). These multidimensional experimental results of alcohol metabolism analysis, righting reflex test, and live injury investigation described above strongly prove the feasibility of AA@mMOF nanoreactor for *in vivo* acute alcoholism treatment to prevent the occurrence of ALI.

***In Vivo* ALI Management.** Compared to acute alcoholism, ALI caused by chronic alcohol consumption is a more serious health problem.[54] Based on the capabilities of alcohol metabolic reprogramming and liver-targeting confirmed above, the AA@mMOF nanoreactor is presumed to possess capability for ALI management. To prove this, a long-term alcohol-fed mouse model (chronic binge drinking), which is more in line with daily human drinking habits and can induce acute-on-chronic liver injury similar to human ALI, was established.[55] AA@mMOF was intravenously injected into the ALI mice after binge drinking, and its therapeutic effect for liver injury was systematically investigated (Figure 6a and Figure S24a). H&E and Oil Red O staining were first performed to show the histological changes of liver tissue of ALI mice in different groups. As shown in Figure 6b and Figure S24b, inflammation and a certain number of lipid droplets (red arrows in H&E staining, and black arrows in Oil Red O staining) were clearly found in the group of no binge compared to the normal healthy mice, indicating chronic liver damage after long-term alcohol drinking. In addition, the number of lipid droplets dramatically increased in the group of PBS compared to that of no binge, demonstrating the massive accumulation of fat as well as fatty liver formation and indicating the successful construction of mouse model of ALI. Moreover, the inflammation and fat accumulation of liver in ALI mice was greatly alleviated after nanoreactor treatment (AA@mMOF, and AA@mMOF + NAD^+), and there was no significant difference in inflammation and lipid droplets number between the group of no binge and the two treatment groups of nanoreactor, demonstrating potential ability to block and reverse the progression of ALI. In addition to histological results of H&E and Oil Red O staining, plasma transaminase concentration and liver oxidative stress level of ALI mice were further analyzed to evaluate the performance of nanoreactor for ALI management. As shown in Figure 6c and Figure S24c, after nanoreactor treatment (AA@mMOF, and AA@mMOF + NAD^+), the elevated plasma ALT and ALT concentration of ALI mice was rapidly reduced to a similar level as that of no binge group compared to the control (PBS), indicating gradual recovery of liver function from ALI. In addition, enhanced SOD activity and GSH concentration as well as reduced MDA, 8-OHdG and triglyceride concentration were observed in the groups of no binge and nanoreactor treatment, demonstrating that liver oxidative stress of ALI mice was efficiently relieved after nanoreactor treatment (Figure 6d, Figures S24d and S25). By effectively reducing fat accumulation and oxidative stress level to restore the function of damaged liver, AA@mMOF nanoreactor shows great promise for *in vivo* ALI management.

Biocompatibility Investigation of AA@mMOF Nanoreactor. The potential biotoxicity of nanomaterials is a major problem limiting their clinical application.[56] By considering the good biocompatibility of the components of MOF and the negligible immunogenicity of enzymes of AOx and ALDH (Figure S26),[57,58] our AA@mMOF nanoreactor has predictable biosafety *in vitro* and *in vivo*. Based on CCK-8 assay and hemolytic analysis, a super high viability of a variety of cell lines including human umbilical vein cells (EA.hy926), mouse mononuclear macrophages (J774) and mouse normal liver cells (AML12) as well as no obvious hemolysis of red blood cells (RBCs) were observed after incubation with AA@mMOF at high concentration (250 μg/mL of mMOF), confirming the excellent *in vitro* biocompatibility of nanoreactor (Figure 2j and Figure S10). To evaluate the biosafety effect of nanoreactor *in vivo*, healthy mice were intravenously injected with AA@mMOF, and *in vivo* pharmacokinetics and tissue distribution of nanoreactor as well as blood transaminase levels, organ histopathological analysis and blood biochemical assay were carried out. As shown in Figure S27, AA@mMOF exhibited a short blood half-life ($t_{1/2}$ = 3.69 ± 0.67 h), demonstrating that the nanoreactor could be rapidly cleared from the blood after intravenous injection without causing blockage of blood vessels. The biodistribution of AA@mMOF in major organs of mice intravenously injected with nanoreactor at different time points postinjection was performed. It was clearly found that AA@mMOF had a super high accumulation in the liver, and this accumulation gradually decreased over time, possessing a typical liver-based metabolic pathway (Figures S28, S29, and S30).[59] The amount of AA@mMOF in the liver dropped to a relatively lower level on the seventh day of nanoreactor postinjection, indicating that most of accumulated nanoreactors had been metabolized to avoid long-term toxicity. In addition, plasma transaminase (ALT and AST) levels of mice intravenously injected with AA@mMOF returned to normal quickly, indicating that the liver function of mice was not affected by the accumulation and metabolism of nanoreactor (Figures S31 and S32). Furthermore, *in vivo* systemic toxicity of AA@mMOF was investigated. From the organ H&E staining images, no lesions and inflammation were found in the main organs of the mice injected with different concentrations of nanoreactor compared to the normal healthy mice without nanoreactor injection (control), indicating the negligible histopathological damage of main organs under nanoreactor administration (Figures S33 and S34). Moreover, there was no obvious difference in blood biochemical indicators measured between the mice injected with different concentrations of nanoreactor and the control, indicating the negligible systemic toxicity and excellent biocompatibility of nanoreactor *in vivo* (Figures S35 and S36). This confirmed *in vitro* and *in vivo* biocompatibility of AA@mMOF nanoreactor lays a solid foundation for its future clinical transformation.

CONCLUSIONS

In summary, by assembling natural enzymes of AOx and ALDH in the porous cavity of MOFs with intrinsic CAT activity, a metabolic reprogramming nanoreactor for targeted alcohol detoxification and ALI management is developed. The confined architecture of nanoreactor can operate high-efficiency AOx/CAT/ALDH cascade reactions and reprogram the metabolic pathway of alcohol. We demonstrate that the nanoreactor can enable self-accelerated alcohol degradation without consumption of NAD^+ and negligible aldehyde accumulation *in vitro*, realizing robust alcohol metabolic reprogramming and significantly reducing the level of intracellular oxidative stress of hepatocytes. Moreover, the nanoreactor shows superior *in vivo* liver targeting and resident properties and can rapidly reverse unconsciousness and acute

https://doi.org/10.1021/acsnano.2c12075
ACS Nano 2023, 17, 7443−7455

liver injury in intoxicated mice, showing great potential in acute alcoholism treatment as an effective antidote. Additionally, the nanoreactor dramatically alleviates fat accumulation and oxidative stress in the liver of intoxicated mice with chronic alcohol consumption, offering a powerful modality for ALI management. The proposed confined cascade metabolic reprogramming strategy provides a paradigm shift for tackling metabolic disorders.

MATERIALS AND METHODS

Materials. Iron(III) chloride hexahydrate ($FeCl_3{\cdot}6H_2O$), 2-aminoterephthalic acid (NH_2-H_2BDC), alcohol oxidase (AOx, derived from *Saccharomyces cerevisiae*), aldehyde dehydrogenase (ALDH, derived from *Saccharomyces cerevisiae*), NH_2-PEG-COOH (M_w = 3500 Da), 3-methyl-2-benzothiazolone hydrazine (MBTH), tetramethyl rhodamine B isothiocyanate (TRITC), fluorescein isothiocyanate (FITC), nicotinamide adenine dinucleotide (NAD^+), dimethyl sulfoxide (DMSO), hydrochloric acid, acetic acid, glutaraldehyde (GA), dimethylformamide (DMF), anhydrous ethanol and cell counting kit-8 (CCK-8) were purchased from Sigma-Aldrich. Alcohol assay kit was obtained from Suzhou Keming Biotechnology Co., Ltd. Hydrogen peroxide (H_2O_2) assay kit and malondialdehyde (MDA) assay kit were obtained from Beyotime Biotechnology. Bicinchoninic acid (BCA) protein assay kit, triglyceride (TG) assay kit, superoxide dismutase (SOD) assay kit, and glutathione (GSH) assay kit were obtained from Nanjing Jiancheng Bioengineering Research Institute. Human umbilical vein cell fusion cells (EA.hy926), mouse mononuclear macrophages (J774), and mouse normal liver cells (AML12) were purchased from American Type Culture Collection (ATCC). All other chemicals were obtained from Adamas-beta and used without further purification. Deionized (DI) water (Millipore Milli-Q grade, 18.2 MΩ) was used in all the experiments.

Preparation of AA@mMOF Nanoreactors. MIL-101 MOF was synthesized according to the previously reported hydrothermal method.[32] In brief, NH_2-H_2BDC (0.2 g) and $FeCl_3{\cdot}6H_2O$ (0.297 g) were dispersed in 20 mL of DMF, then 5.5 mmol acetic acid was added to the solution and sonicated for 15 min. Subsequently, the mixed solution was transferred to a Teflon-lined autoclave and reacted at 150 °C for 4 h. The MOF precipitate was collected by centrifugation and dried under vacuum at 80 °C overnight. The synthesized MOF powder (30 mg) was then dispersed in 10 mL of DMF solution containing 100 μmol/L of hydrochloric acid, transferred to a Teflon-lined autoclave and reacted at 70 °C to perform acid etching. After 30 min reaction, the mMOF precipitate with mesoporous structure was collected by centrifugation. The as-prepared mMOF (4 mg) dissolved in 2 mL of PBS was mixed with 80 μL of glutaraldehyde solution and was stirred for 6 h at room temperature to prepare activated mMOF. For enzyme loading, AOx (200 μg) and ALDH (600 μg) were mixed with 1 mL of the activated mMOF solution (1 mg/mL) and stirred overnight under ice bath conditions. Finally, 3.5 mg of NH_2-PEG-COOH was added into the mixed solution and stirred overnight to prepare AA@mMOF nanoreactors. After centrifugation, the AA@mMOF nanoreactors were collected and stored in PBS for further characterization.

Preparation of Fluorescent AA@mMOF Nanoreactor. The FITC-labeled AOx (AOx-FITC) and TRITC-labeled ALDH (ALDH-TRITC) were first synthesized according to the experimental procedures previously reported.[60] In brief, FITC and TRITC were dissolved in anhydrous DMSO to obtain a stock solution at a concentration of 10 mg/mL, respectively. Then 50 μL of FITC and TRITC were added drop by drop to 2 mL of AOx and ALDH solutions (10 mg/mL protein, pH 8.2, sodium carbonate buffer), respectively. After overnight reaction at 4 °C, the labeled proteins were dialyzed in a phosphate buffer (20 mM, pH = 7) and finally concentrated and collected through ultrafiltration centrifuge. By using the prepared AOx-FITC and ALDH-TRITC as the constituent enzymes, the fluorescent AA@mMOF nanoreactor was obtained based on the same method employed in nonfluorescent nanoreactor preparation described above.

FRET Assay of Fluorescent AA@mMOF Nanoreactor. To demonstrate the close association of AOx and ALDH in the fluorescent AA@mMOF nanoreactor, the fluorescence spectrum and confocal fluorescence microscope image of AA@mMOF loaded with AOx-FITC and ALDH-TRITC were recorded under the excitation of 450 and 488 nm, respectively, to demonstrate the occurrence of FRET between FITC and TRITC. The fluorescence spectrum of the mixture of AOx-FITC + ALDH-TRITC (the ratio of AOx-FITC to ALDH-TRITC was 1:3) under 450 nm excitation was measured and used as the control.

AOx Activity Evaluation of AA@mMOF Nanoreactor. The AOx activity of AA@mMOF under different adverse environmental influences (protease K, weak acid with pH 5.5, and heat with 37 °C temperature) was evaluated by measuring the generation rate of aldehyde in the presence of alcohol, based on the chromogenic reaction between aldehyde and MBTH. In brief, AA@mMOF solution (250 μg/mL of mMOF) treated by protease K, weak acid with pH 5.5, and heat with 37 °C temperature was first reacted with alcohol (0.1%, w/v) for 5 min at room temperature, respectively. The reaction mixture was then incubated with MBTH (0.5%, w/v) for 15 min in the presence of ferric chloride to form a blue product with absorbance around 600 nm, and the AOx activity of AA@mMOF nanoreactor was determined by analyzing the formation of blue product.

***In Vitro* biocompatibility assay.** The biocompatibility of AA@mMOF nanoreactors was determined by CCK-8 assay and hematolysis test.[61] In the CCK-8 assay, human umbilical vein cell fusion cells (EA.hy926), mouse mononuclear macrophages (J774), and mouse normal liver cells (AML12) were seeded onto 96-well plate (8000−10,000 cells/well) and cultured overnight, respectively. Subsequently, cells were incubated with AA@mMOF at different concentrations (0, 50, 100, 150, 200, and 250 μg/mL of mMOF) for 24 h. CCK-8 reagent was finally added and cultured for another 2 h, and cells' viability was obtained by microplate reader.

In the hematolysis test, diluted red blood cells extracted from the blood of healthy mice were incubated with different concentrations (15.625, 31.25, 62.5, 125, and 250 μg/mL of mMOF) of AA@mMOF nanoreactor for 4 h at 37 °C and centrifuged at 2000 rpm for 10 min. Afterwards, the absorbance of the supernatant at 570 nm was measured using a microplate reader. Red blood cells in DI water and PBS were used as the positive and negative control, respectively.

Alcohol Metabolism in AA@mMOF Nanoreactor. To investigate the alcohol metabolism in the AA@mMOF nanoreactor, alcohol solution (1 mg/mL) was mixed with nanoreactor in the presence of 100 μg/mL of NAD^+, and its metabolism process was analyzed by monitoring the degradation of alcohol, the accumulation of aldehyde, the elimination of H_2O_2, and the generation of O_2 in real time. The degradation of alcohol was determined by the alcohol assay kit, and the accumulation of aldehyde concentration was determined by the chromogenic reaction between aldehyde and MBTH. The elimination of H_2O_2 was determined by the H_2O_2 assay kit, and the generation of oxygen was measured using a dissolved oxygen meter. In above alcohol metabolism process, the groups of PBS, and the mixture of AOx and ALDH were used as the controls.

***In Vitro* Alcohol Detoxification.** Alcohol (50 mM)-stimulated AML12 cells were incubated with AA@mMOF nanoreactor (with or without 100 μg/mL of NAD^+) for 24 h. After incubation, AML12 cells were lysed, and the SOD activity and the concentrations of GSH and MDA in the lysate were determined using the corresponding detection kits to assess the intracellular oxidative stress of alcohol-stimulated AML12 cells after nanoreactor treatment. In addition, the viability of a variety of alcohol-stimulated cells including AML12, J774, and EA.hy926 after 24 h incubation of AA@mMOF nanoreactor (with or without 100 μg/mL of NAD^+) was detected based on CCK-8 assay. In above experiments, the groups of PBS and normal healthy mice were used as the controls.

Establishment of Mouse Model of Acute Alcoholism. Female Balb/c and male C57BL/6J mice (7 weeks) were purchased from

https://doi.org/10.1021/acsnano.2c12075
ACS Nano 2023, 17, 7443−7455

Jinan Pengyue Experimental Animal Breeding Co., Ltd. and employed to establish the mouse model of acute alcoholism. Compared to Balb/c mice, C57BL/6J mice were more preferable due to their lower aversion to alcohol, and the sex of mice was fixed to exclude the effect of sex on the performance of nanoreactor.[62] All animal experiments were conducted in accordance with the procedures approved by the Experimental Animal Center of Shandong University. To establish the model of acute alcoholism, mice fasted for 12 h and then were administered large amounts of alcohol (6 mg/g body weight) via gavage to trigger acute alcoholism.

***In Vivo* Treatment of Acute Alcoholism.** The mice with acute alcoholism were divided into three treatment groups including PBS (positive control), AA@mMOF, and AA@mMOF plus NAD^+, while the group of normal healthy mice was used as the negative control. Each treatment group contained 6−10 mice. To perform *in vivo* acute alcoholism treatment, intoxicated mice (Female Balb/c and male C57BL/6J) were treated by intravenously injecting nanoreactor (12.5 mg/kg of mMOF) at the 0.25 h postgavage of alcohol through the tail vein. The blood concentrations of alcohol and aldehyde of intoxicated mice in different treatment groups were measured every 2 h within 8 h treatment to analyze the metabolism of alcohol analysis. Meanwhile, *ex vivo* organ fluorescence images of intoxicated mice were recorded to study the *in vivo* distribution of nanoreactor. In addition, the righting reflex test was employed to investigate the recovery of consciousness of intoxicated mice after treatment. At 9 h postgavage of alcohol, the intoxicated mice in all treatment groups were sacrificed, and liver histological condition (H&E staining) as well as plasma transaminase (ALT and AST) levels and liver oxidative indicators (SOD activity, MDA and GSH concentration) were measured and analyzed to evaluate the performance of nanoreactor for acute liver injury treatment.

***In Vivo* Management of ALI.** To better mirror the human ALI, a long-term alcohol-fed mouse model (chronic binge drinking), which is more in line with daily human drinking habits and can induce a liver injury similar to human ALI, was established by employing the method of National Institute on Alcohol Abuse and Alcoholism (NIAAA) previously reported.[55] Briefly, female Balb/c and male C57BL/6J mice (7 weeks) were first acclimated to a liquid diet (a nonalcoholic liquid diet with maltose as the main ingredient) for 5 days and then fed an alcohol-containing liquid diet (5% alcohol, chronic drinking) and a single high-dose of alcohol (6 mg/g body weight, binge drinking) sequentially, to approximate acute-on-chronic liver injury in ALI patients. For *in vivo* ALI management, the ALI mice were treated with AA@mMOF (12.5 mg/kg of mMOF) at the 0.25 h postgavage of high-dose of alcohol through the tail vein. Three treatment groups including PBS, AA@mMOF, and AA@mMOF plus NAD^+ were divided, while the groups of normal healthy mice and no binge were used the controls. Each treatment group contained 6−10 mice. Nine h later, the ALI mice in all groups were sacrificed, and liver histological condition (H&E and Oil Red O staining) as well as plasma transaminase (ALT and AST) levels and liver oxidative indicators (SOD activity, the concentrations of MDA, GSH and TG) were measured and analyzed to evaluate the performance of nanoreactor for ALI management.

ASSOCIATED CONTENT

Supporting Information

The Supporting Information is available free of charge at https://pubs.acs.org/doi/10.1021/acsnano.2c12075.

XPS spectra of MOF and nanoreactor; N_2 absorption/desorption isotherms of MOF before and after etching; XRD spectra of MOF before and after etching; BCA assay; hydrodynamic size; CLSM images and fluorescence intensity curves of AOx-FITC and ALDH-TRITC; stability of nanoreactor; AOx activity investigation; hemolysis test; XPS spectrum of nanoreactor; optical pH of AOx, ALDH and CAT; aldehyde generation assay; cellular uptake mechanism and intracellular localization of nanoreactor; *in vivo* performance of AA@mMOF nanoreactor for acute alcoholism treatment and ALI management in Balb/c mice; blood pharmacokinetics, *in vivo* tissue biodistribution and systemic toxicity evaluation of AA@mMOF nanoreactor (PDF)

Video S1: (MP4)

Video S2: (MP4)

AUTHOR INFORMATION

Corresponding Authors

Kangsheng Tu − *Department of Hepatobiliary Surgery, the First Affiliated Hospital of Xi'an Jiaotong University, Xi'an 710061, China*; Email: tks0912@foxmail.com

Yong-Qiang Li − *Institute of Advanced Interdisciplinary Science, School of Physics, Shandong University, Jinan 250100, China*; orcid.org/0000-0003-1551-3020; Email: yqli@sdu.edu.cn

Authors

Xudong Geng − *Institute of Advanced Interdisciplinary Science, School of Physics, Shandong University, Jinan 250100, China*

Xuancheng Du − *Institute of Advanced Interdisciplinary Science, School of Physics, Shandong University, Jinan 250100, China*

Weijie Wang − *Institute of Advanced Interdisciplinary Science, School of Physics, Shandong University, Jinan 250100, China*

Chengmei Zhang − *Laboratory Animal Center of Shandong University, Jinan 250012, China*

Xiangdong Liu − *Institute of Advanced Interdisciplinary Science, School of Physics, Shandong University, Jinan 250100, China*

Yuanyuan Qu − *Institute of Advanced Interdisciplinary Science, School of Physics, Shandong University, Jinan 250100, China*; orcid.org/0000-0001-9134-3567

Mingwen Zhao − *Institute of Advanced Interdisciplinary Science, School of Physics, Shandong University, Jinan 250100, China*; orcid.org/0000-0002-7583-9682

Weifeng Li − *Institute of Advanced Interdisciplinary Science, School of Physics, Shandong University, Jinan 250100, China*; orcid.org/0000-0002-0244-2908

Mingzhen Zhang − *School of Basic Medical Sciences, Xi'an Key Laboratory of Immune Related Diseases, Xi'an Jiaotong University, Xi'an 710061, China*; orcid.org/0000-0002-4686-6526

Complete contact information is available at: https://pubs.acs.org/10.1021/acsnano.2c12075

Author Contributions

#X. Geng and X. Du contributed equally to this work.

Notes

The authors declare no competing financial interest.

ACKNOWLEDGMENTS

This work was supported by the National Natural Science Foundation of China (31500802, 82000523), the Natural Science Foundation of Jiangsu Province (BK20190097), and the Program of Qilu Young Scholars of Shandong University. This work was also supported by the Huadong Medicine Joint Funds of the Zhejiang Provincial Natural Science Foundation of China (LHDMD23H300002), Cyrus Tang Foundation, the

Taishan Scholars Program for Young Expert of Shandong Province (tsqn201909021), and the Youth cross-scientific innovation group of Shandong University.

REFERENCES

(1) Carvalho, A. F.; Heilig, M.; Perez, A.; Probst, C.; Rehm, J. Alcohol Use Disorders. *Lancet* **2019**, *394*, 781−792.
(2) Niu, L. L.; Thiele, M.; Geyer, P. E.; Rasmussen, D. N.; Webel, H. E.; Santos, A.; Gupta, R.; Meier, F.; Strauss, M.; Kjaergaard, M.; Lindvig, K.; Jacobsen, S.; Rasmussen, S.; Hansen, T.; Krag, A.; Mann, M. Noninvasive Proteomic Biomarkers for Alcohol-Related Liver Disease. *Nat. Med.* **2022**, *28*, 1277−1287.
(3) White, A. M.; Castle, I. J. P.; Powell, P. A.; Hingson, R. W.; Koob, G. F. Alcohol-Related Deaths During the COVID-19 Pandemic. *JAMA* **2022**, *327*, 1704−1706.
(4) Rumgay, H.; Shield, K.; Charvat, H.; Ferrari, P.; Sornpaisarn, B.; Obot, I.; Islami, F.; Lemmens, V. E. P. P.; Rehm, J.; Soerjomataram, I. Global Burden of Cancer in 2020 Attributable to Alcohol Consumption: A Population-Based Study. *Lancet Oncol.* **2021**, *22*, 1071−1080.
(5) Shield, K.; Manthey, J.; Rylett, M.; Probst, C.; Wettlaufer, A.; Parry, C. D. H.; Rehm, J. National, Regional, and Global Burdens of Disease from 2000 to 2016 Attributable to Alcohol Use: A Comparative Risk Assessment Study. *Lancet Public Health* **2020**, *5*, e51−e61.
(6) Drummond, D. C.; Thom, B.; Brown, C.; Edwards, G.; Mullan, M. J. Specialist Versus General-Practitioner Treatment of Problem Drinkers. *Lancet* **1990**, *336*, 915−918.
(7) Ding, M.; Boyd, A.; Parker, C.; Towey, J.; Harborne, M.; Ngonadi, C.; Magrabi, M.; Hopkins, L. J.; Thompson, T.; Bansal, S.; Morris, S.; Mohideen, A.; Harrison, A.; Catling, J.; Webb, K.; Holt, A.; Rajoriya, N. Specialist Mdt Clinic Improves Transplant Outcomes of High Risk Patients with Alcohol-Related Liver Disease. *Hepatology* **2019**, *70*, 680a.
(8) Joenje, H. METABOLISM Alcohol, DNA and Disease. *Nature* **2011**, *475*, 45−46.
(9) Feinman, L.; Lieber, C. S. Ethanol and Lipid Metabolism. *Am. J. Clin. Nutr.* **1999**, *70*, 791−792.
(10) Wall, T. L.; Peterson, C. M.; Peterson, K. P.; Johnson, M. L.; Thomasson, H. R.; Cole, M.; Ehlers, C. L. Alcohol Metabolism in Asian-American Men with Genetic Polymorphisms of Aldehyde Dehydrogenase. *Ann. Int. Med.* **1997**, *127*, 376−379.
(11) Cederbaum, A. I. Alcohol Metabolism. *Clin. Liver Dis.* **2012**, *16*, 667−685.
(12) Shcherban, N. D.; Diyuk, O. A.; Zazhigalov, V. A.; Murzin, D. Y. Graphitic Carbon Nitride as a Sustainable Catalyst for Selective Ethanol Oxidation. *ACS Sustainable Chem. Eng.* **2021**, *9*, 5128−5137.
(13) Tarantino, G.; Cataldi, M.; Citro, V. Could Alcohol Abuse and Dependence on Junk Foods Inducing Obesity and/or Illicit Drug Use Represent Danger to Liver in Young People with Altered Psychological/Relational Spheres or Emotional Problems? *Int. J. Mol. Sci.* **2022**, *23*, 10406.
(14) Massart, J.; Begriche, K.; Hartman, J. H.; Fromenty, B. Role of Mitochondrial Cytochrome P450 2E1 in Healthy and Diseased Liver. *Cell* **2022**, *11*, 288.
(15) Kato, S.; Alderman, J.; Lieber, C. S. The Microsomal Ethanol Oxidizing System (MEOS) Accounts for Ethanol-Metabolism after Chronic Ethanol Treatment in Deermouse Hepatocytes Lacking Alcohol-Dehydrogenase (ADH). *Hepatology* **1987**, *7*, 1042.
(16) French, S. W.; Takahashi, H.; Johansson, I.; Ingelmansundberg, M. Effect of the Type of Dietary-Fat and Ethanol on MEOS, Alcohol Inducible Cytochrome-P450 and Para-Nitrophenol Hydroxylase-Activity. *Hepatology* **1990**, *12*, 979.
(17) Xu, D.; Han, H.; He, Y.; Lee, H.; Wu, D.; Liu, F.; Liu, X.; Liu, Y.; Lu, Y.; Ji, C. A Hepatocyte-Mimicking Antidote for Alcohol Intoxication. *Adv. Mater.* **2018**, *30*, 1707443.
(18) Liu, Y.; Du, J.; Yan, M.; Lau, M. Y.; Hu, J.; Han, H.; Yang, O. O.; Liang, S.; Wei, W.; Wang, H.; Li, J.; Zhu, X.; Shi, L.; Chen, W.; Ji, C.; Lu, Y. Biomimetic Enzyme Nanocomplexes and Their Use as Antidotes and Preventive Measures for Alcohol Intoxication. *Nat. Nanotechnol.* **2013**, *8*, 187−192.
(19) Cai, S.; Liu, J.; Ding, J.; Fu, Z.; Li, H.; Xiong, Y.; Lian, Z.; Yang, R.; Chen, C. Tumor-Microenvironment-Responsive Cascade Reactions by a Cobalt-Single-Atom Nanozyme for Synergistic Nanocatalytic Chemotherapy. *Angew. Chem., Int. Ed.* **2022**, *61*, e2022045.
(20) Phua, S. Z. F.; Yang, G.; Lim, W. Q.; Verma, A.; Chen, H.; Thanabalu, T.; Zhao, Y. Catalase-Integrated Hyaluronic Acid as Nanocarriers for Enhanced Photodynamic Therapy in Solid Tumor. *ACS Nano* **2019**, *13*, 4742−4751.
(21) Du, X.; Zhang, M.; Zhou, H.; Wang, W.; Zhang, C.; Zhang, L.; Qu, Y.; Li, W.; Liu, X.; Zhao, M.; Tu, K.; Li, Y. Decoy Nanozymes Enable Multitarget Blockade of Proinflammatory Cascades for the Treatment of Multi-Drug-Resistant Bacterial Sepsis. *Research* **2022**, *2022*, 9767643.
(22) Yang, X.; Yi, J.; Wang, T.; Feng, Y.; Wang, J.; Yu, J.; Zhang, F.; Jiang, Z.; Lv, Z.; Li, H.; Huang, T.; Si, D.; Wang, X.; Cao, R.; Chen, X. Wet-Adhesive On-Skin Sensors Based on Metal-Organic Frameworks for Wireless Monitoring of Metabolites in Sweat. *Adv. Mater.* **2022**, *34*, 2201768.
(23) Wang, X.; Xu, W.; Gu, J.; Yan, X.; Chen, Y.; Guo, M.; Zhou, G.; Tong, S.; Ge, M.; Liu, Y.; Chen, C. MOF-Based Fibrous Membranes Adsorb PM Efficiently and Capture Toxic Gases Selectively. *Nanoscale* **2019**, *11*, 17782−17790.
(24) Liu, Y.; Wang, H.; Shi, W.; Zhang, W.; Yu, J.; Chandran, B. K.; Cui, C.; Zhu, B.; Liu, Z.; Li, B.; Xu, C.; Xu, Z.; Li, S.; Huang, W.; Huo, F.; Chen, X. Alcohol-Mediated Resistance-Switching Behavior in Metal-Organic Framework-Based Electronic Devices. *Angew. Chem., Int. Ed.* **2016**, *55*, 8884−8888.
(25) Wang, Z.; Liu, B.; Sun, Q.; Feng, L.; He, F.; Yang, P.; Gai, S.; Quan, Z.; Lin, J. Upconverted Metal-Organic Framework Janus Architecture for Near-Infrared and Ultrasound Co-Enhanced High Performance Tumor Therapy. *ACS Nano* **2021**, *15* (7), 12342−12357.
(26) Liu, X.; Yan, Z.; Zhang, Y.; Liu, Z.; Sun, Y.; Ren, J.; Qu, X. Two-Dimensional Metal−Organic Framework/Enzyme Hybrid Nanocatalyst as a Benign and Self-Activated Cascade Reagent for *In Vivo* Wound Healing. *ACS Nano* **2019**, *13*, 5222−5230.
(27) Pattipeiluhu, R.; Arias-Alpizar, G.; Basha, G.; Chan, K. Y. T.; Bussmann, J.; Sharp, T. H.; Moradi, M. A.; Sommerdijk, N.; Harris, E. N.; Cullis, P. R.; Kros, A.; Witzigmann, D.; Campbell, F. Anionic Lipid Nanoparticles Preferentially Deliver mRNA to the Hepatic Reticuloendothelial System. *Adv. Mater.* **2022**, *34*, 2201095.
(28) Tang, Y.; Wang, X.; Li, J.; Nie, Y.; Liao, G.; Yu, Y.; Li, C. Overcoming the Reticuloendothelial System Barrier to Drug Delivery with a "Don't-Eat-Us" Strategy. *ACS Nano* **2019**, *13*, 13015−13026.
(29) Lan, G.; Ni, K.; Xu, Z.; Veroneau, S. S.; Song, Y.; Lin, W. Nanoscale Metal-Organic Framework Overcomes Hypoxia for Photodynamic Therapy Primed Cancer Immunotherapy. *J. Am. Chem. Soc.* **2018**, *140*, 5670−5673.
(30) Xiong, Y.; Tsitkov, S.; Hess, H.; Gang, O.; Zhang, Y. Microscale Colocalization of Cascade Enzymes Yields Enhancement. *ACS Nano* **2022**, *16*, 10383−10391.
(31) Wang, T.; Lei, Q.; Wang, M.; Deng, G.; Yang, L.; Liu, X.; Li, C.; Wang, Q.; Liu, Z.; Wang, J.; Cui, Z.; Utama, K. G.; Ni, R.; Chen, X. Mechanical Tolerance of Cascade Bioreactions via Adaptive Curvature Engineering for Epidermal Bioelectronics. *Adv. Mater.* **2020**, *32*, 2000991.
(32) Yin, X.; Yang, B.; Chen, B.; He, M.; Hu, B. Multifunctional Gold Nanocluster Decorated Metal-Organic Framework for Real-Time Monitoring of Targeted Drug Delivery and Quantitative Evaluation of Cellular Therapeutic Response. *Anal. Chem.* **2019**, *91*, 10596−10603.
(33) Yao, Y.; Jin, Y.; Jia, X.; Yang, Y. Construction of Hyaluronic Acid-Covered Hierarchically Porous MIL-nanoMOF for Loading and Controlled Release of Doxorubicin. *Chem.—Eur. J.* **2021**, *27*, 2987−2992.

https://doi.org/10.1021/acsnano.2c12075
ACS Nano 2023, 17, 7443−7455

(34) Mayorga-Martinez, C. C.; Sofer, Z.; Pumera, M. Binary Phosphorene Redox Behavior in Oxidoreductase Enzymatic Systems. *ACS Nano* **2019**, *13*, 13217−13224.
(35) Du, X.; Jia, B.; Wang, W.; Zhang, C.; Liu, X.; Qu, Y.; Zhao, M.; Li, W.; Yang, Y.; Li, Y. pH-Switchable Nanozyme Cascade Catalysis: A Strategy for Spatial-Temporal Modulation of Pathological Wound Microenvironment to Rescue Stalled Healing in Diabetic Ulcer. *J. Nanobiotechnol.* **2022**, *20*, 12.
(36) Russell, R. J.; Pishko, M. V.; Gefrides, C. C.; McShane, M. J.; Cote, G. L. A Fluorescence-Based Glucose Biosensor Using Concanavalin A and Dextran Encapsulated in a Poly(Ethylene Glycol) Hydrogel. *Anal. Chem.* **1999**, *71*, 3126−3132.
(37) Algar, W. R.; Hildebrandt, N.; Vogel, S. S.; Medintz, I. L. FRET as a Biomolecular Research Tool-Understanding Its Potential While Avoiding Pitfalls. *Nat. Methods* **2019**, *16*, 815−829.
(38) Zhao, Z.; Yan, R.; Yi, X.; Li, J.; Rao, J.; Guo, Z.; Yang, Y.; Li, W.; Li, Y.; Chen, C. Bacteria-Activated Theranostic Nanoprobes against Methicillin-Resistant Staphylococcus aureus Infection. *ACS Nano* **2017**, *11*, 4428−4438.
(39) Xia, H.; Li, N.; Huang, W.; Song, Y.; Jiang, Y. Enzymatic Cascade Reactions Mediated by Highly Efficient Biomimetic Quasi Metal-Organic Frameworks. *ACS Appl. Mater. Interfaces* **2021**, *13*, 22240−22253.
(40) Billington, R. A.; Bruzzone, S.; De Flora, A.; Genazzani, A. A.; Koch-Nolte, F.; Ziegler, M.; Zocchi, E. Emerging Functions of Extracellular Pyridine Nucleotides. *Mol. Med.* **2006**, *12*, 324−327.
(41) Stephens, A. N.; Bishop, C. A.; Liu, S.; Fitzharris, M. Alcohol Consumption Patterns and Attitudes Toward Drink-Drive Behaviours and Road Safety Enforcement Strategies. *Accid. Anal. Prev.* **2017**, *98*, 241−251.
(42) Wrzosek, L.; Ciocan, D.; Hugot, C.; Spatz, M.; Dupeux, M.; Houron, C.; Lievin-Le Moal, V.; Puchois, V.; Ferrere, G.; Trainel, N.; Mercier-Nome, F.; Durand, S.; Kroemer, G.; Voican, C. S.; Emond, P.; Straube, M.; Sokol, H.; Perlemuter, G.; Cassard, A. M. Microbiota Tryptophan Metabolism Induces Aryl Hydrocarbon Receptor Activation and Improves Alcohol-Induced Liver Injury. *Gut* **2021**, *70*, 1299−1308.
(43) Kalyanaraman, B. Teaching the Basics of Redox Biology to Medical and Graduate Students: Oxidants, Antioxidants and Disease Mechanisms. *Redox Biology* **2013**, *1*, 244−257.
(44) Weismann, D.; Hartvigsen, K.; Lauer, N.; Bennett, K. L.; Scholl, H. P. N.; Issa, P. C.; Cano, M.; Brandstatter, H.; Tsimikas, S.; Skerka, C.; Superti-Furga, G.; Handa, J. T.; Zipfel, P. F.; Witztum, J. L.; Binder, C. J. Complement Factor H Binds Malondialdehyde Epitopes and Protects from Oxidative Stress. *Nature* **2011**, *478*, 76−81.
(45) Hsieh, Y. W.; Lin, K. C.; Korivi, M.; Lee, T. H.; Wu, C. Y.; Wu, K. Y. The Reliability and Predictive Ability of A Biomarker of Oxidative DNA Damage on Functional Outcomes after Stroke Rehabilitation. *Int. J. Mol. Sci.* **2014**, *15*, 6504−6516.
(46) Cambronne, X. A.; Stewart, M. L.; Kim, D.; Jones-Brunette, A. M.; Morgan, R. K.; Farrens, D. L.; Cohen, M. S.; Goodman, R. H. Biosensor Reveals Multiple Sources for Mitochondrial NAD(+). *Science* **2016**, *352*, 1474−1477.
(47) Lehtinen, M. K.; Yuan, Z.; Boag, P. R.; Yang, Y.; Villen, J.; Becker, E. B. E.; DiBacco, S.; de la Iglesia, N.; Gygi, S.; Blackwell, T. K.; Bonni, A. A Conserved MST-FOXO Signaling Pathway Mediates Oxidative-Stress Responses and Extends Life Span. *Cell* **2006**, *125*, 987−1001.
(48) Cunningham, C. L.; Fidler, T. L.; Murphy, K. V.; Mulgrew, J. A.; Smitasin, P. J. Time-Dependent Negative Reinforcement of Ethanol Intake by Alleviation of Acute Withdrawal. *Biol. Psychiatry* **2013**, *73*, 249−255.
(49) Protzer, U.; Maini, M. K.; Knolle, P. A. Living in the Liver: Hepatic Infections. *Nat. Rev. Immunol.* **2012**, *12*, 201−213.
(50) Tsoi, K. M.; MacParland, S. A.; Ma, X.; Spetzler, V. N.; Echeverri, J.; Ouyang, B.; Fadel, S. M.; Sykes, E. A.; Goldaracena, N.; Kaths, J. M.; Conneely, J. B.; Alman, B. A.; Selzner, M.; Ostrowski, M. A.; Adeyi, O. A.; Zilman, A.; McGilvray, I. D.; Chan, W. C. W. Mechanism of Hard-Nanomaterial Clearance by the Liver. *Nat. Mater.* **2016**, *15*, 1212−1221.
(51) Shi, J. L.; Kokubo, Y.; Wake, K. Expression of P-selectin on Hepatic Endothelia and Platelets Promoting Neutrophil Removal by Liver Macrophages. *Blood* **1998**, *92*, 520−528.
(52) Radcliffe, R. A.; Bludeau, P.; Deng, X.; Erwin, V. G.; Deitrich, R. A. Short-Term Selection for Acute Ethanol Tolerance and Sensitization from an F-2 Population Derived from the High and Low Alcohol-Sensitive Selectively Bred Rat Lines. *Alcohol* **2007**, *41*, 557−566.
(53) Arteel, G. E. Liver-Lung Axes in Alcohol-Related Liver Disease. *Clin. Mol. Hepatol.* **2020**, *26*, 670−676.
(54) Tao, H.; Guo, J.; Ma, Y.; Zhao, Y.; Jin, T.; Gu, L.; Dou, Y.; Liu, J.; Hu, H.; Xiong, X.; Zhang, J. Luminescence Imaging of Acute Liver Injury by Biodegradable and Biocompatible Nanoprobes. *ACS Nano* **2020**, *14*, 11083−11099.
(55) Bertola, A.; Mathews, S.; Ki, S. H.; Wang, H.; Gao, B. Mouse Model of Chronic and Binge Ethanol Feeding (the NIAAA Model). *Nat. Protoc.* **2013**, *8*, 627−637.
(56) Wang, J.; Chen, X.; Zhao, Y.; Yang, Y.; Wang, W.; Wu, C.; Yang, B.; Zhang, Z.; Zhang, L.; Liu, Y.; Du, X.; Li, W.; Qiu, L.; Jiang, P.; Mou, X.; Li, Y. pH-Switchable Antimicrobial Nanofiber Networks of Hydrogel Eradicate Biofilm and Rescue Stalled Healing in Chronic Wounds. *ACS Nano* **2019**, *13*, 11686−11697.
(57) Du, Y.; Jia, X.; Zhong, L.; Jiao, Y.; Zhang, Z.; Wang, Z.; Feng, Y.; Bilal, M.; Cui, J.; Jia, S. Metal-Organic Frameworks with Different Dimensionalities: An Ideal Host Platform for Enzyme@MOF Composites. *Coord. Chem. Rev.* **2022**, *454*, 214327.
(58) Costa, I. M.; Schultz, L.; Pedra, B. D. B.; Leite, M. S. M.; Farsky, S. H. P.; de Oliveira, M. A.; Pessoa, A.; Monteiro, G. Recombinant L-asparaginase 1 from Saccharomyces Cerevisiae: an Allosteric Enzyme with Antineoplastic Activity. *Sci. Rep.* **2016**, *6*, 36239.
(59) Bechmann, L. P.; Hannivoort, R. A.; Gerken, G.; Hotamisligil, G. S.; Trauner, M.; Canbay, A. The Interaction of Hepatic Lipid and Glucose Metabolism in Liver Diseases. *J. Hepatol.* **2012**, *56*, 952−964.
(60) Chen, W.; Vazquez-Gonzalez, M.; Zoabi, A.; Abu-Reziq, R.; Willner, I. Biocatalytic Cascades Driven by Enzymes Encapsulated in Metal-Organic Framework Nanoparticles. *Nat. Catal.* **2018**, *1*, 689−695.
(61) Wang, J.; Wu, H.; Yang, Y.; Yan, R.; Zhao, Y.; Wang, Y.; Chen, A.; Shao, S.; Jiang, P.; Li, Y. Bacterial Species-Identifiable Magnetic Nanosystems for Early Sepsis Diagnosis and Extracorporeal Photodynamic Blood Disinfection. *Nanoscale* **2018**, *10*, 132−141.
(62) Wilkin, R. J. W.; Lalor, R. F.; Parker, R.; Newsome, P. N. Murine Models of Acute Alcoholic Hepatitis and Their Relevance to Human Disease. *Am. J. Pathol.* **2016**, *186*, 748−760.

https://doi.org/10.1021/acsnano.2c12075
ACS Nano 2023, 17, 7443−7455